Bull Volcanol (2016) 78: 66
DOI 10.1007/s00445-016-1059-7

RESEARCH ARTICLE

Dispersal of key subplinian–Plinian tephras from Hekla volcano, Iceland: implications for eruption source parameters

Maria H. Janebo[1,2] · Thorvaldur Thordarson[3] · Bruce F. Houghton[1] · Costanza Bonadonna[4] · Gudrun Larsen[5] · Rebecca J. Carey[6]

Received: 7 September 2015 / Accepted: 11 August 2016 / Published online: 6 September 2016

Abstract Hekla is the most active silicic volcano in Iceland, with 18 subplinian–Plinian eruptions since AD 1104. In the period 1970 to 2000, the frequency of such eruptions increased to once every decade. Hekla is currently inflated to above the levels observed prior to the most recent eruptions in 1991 and 2000. The next eruption could pose a hazard to air traffic between North America and Europe because explosive eruptions of Hekla, independent of size, typically start with a subplinian or Plinian phase that produces a sustained ash plume. We present an overview of five of the largest historical Hekla eruptions (taking place in 1104, 1158, 1300, 1693, and 1766). These eruptions cover a compositional range of rhyolite to andesite, previously estimated Volcanic Explosivity Index (VEI) values of 4–5 and are characterised by contrasting wind dispersal (dispersal axes NW–NE). New isopach maps show both greater deposit thicknesses in the proximal region and wider dispersal than previously inferred, resulting in different volume estimates (minimal values ranging between 0.18 and 0.91 km^3). New isopleth maps were also compiled and resulted in inferred plume heights of about 13–25 km. These changes in the estimated values of volume and mass eruption rates have large implications on the forecasting and impacts of future Hekla eruptions.

Keywords Hekla volcano · Isopach maps · Tephra dispersal · Eruptive volume · Mass eruption rate · Plinian eruptions

Editorial responsibility: J. Fierstein

Electronic supplementary material The online version of this article (doi:10.1007/s00445-016-1059-7) contains supplementary material, which is available to authorized users.

✉ Maria H. Janebo
janebo@hawaii.edu

[1] Department of Geology and Geophysics, SOEST, University of Hawai'i at Mānoa, Honolulu, USA

[2] Present address: Nordic Volcanological Center, Institute of Earth Sciences, University of Iceland, Reykjavik, Iceland

[3] Faculty of Earth Sciences, University of Iceland, Reykjavik, Iceland

[4] Section of Earth and Environmental Sciences, University of Geneva, Geneva, Switzerland

[5] Institute of Earth Sciences, University of Iceland, Reykjavik, Iceland

[6] School of Earth Science, University of Tasmania, Hobart, Australia

Introduction

Hekla is a ridge-shaped stratovolcano, located in the East Volcanic Zone in Iceland. It is the central volcano for the Hekla-Vatnafjöll volcanic system which is 60 km long and 19 km wide, covering an area of 720 km^2 (Thordarson and Höskuldsson 2008). Hekla has erupted explosively 18 times since Iceland was settled (~AD 870), making it the country's second most frequently historically active volcano (Thordarson and Larsen 2007), as well as one of the most active subplinian–Plinian volcanoes in the world. Between 1970 and 2000, the eruption frequency increased to once per decade and Hekla is currently inflated to above the levels observed prior to the two most recent eruptions in 1991 and 2000 (Sturkell et al. 2013).

The historical activity of Hekla covers a range of eruptive styles, intensities and magma compositions. Activity has included effusive, violent Strombolian, subplinian and Plinian episodes. The silica content of the initial magma, and the intensity of the opening phase, increases with increasing repose period (Thorarinsson 1967). The eruptions start with either a Plinian or subplinian (intermediate) phase from the summit, which generally is followed by Strombolian activity

as well as lava emission (Thorarinsson 1967; Thordarson and Höskuldsson 2008). During most Hekla eruptions, a SW–NE trending fissure opens up along the crest of the volcano, and occasionally radial fissures open up on the flanks (Thordarson and Larsen 2007 and references therein). The high eruption frequency, in combination with the fact that all the historical eruptions—independent of size and magma composition—started with a powerful explosive phase that formed a sustained ash plume up to 12–36 km (Thorarinsson 1967), makes future eruptions of Hekla a likely threat to European and transatlantic air traffic, especially between North America and Europe (e.g. Biass et al. 2014b; Scaini et al. 2014).

For these reasons, Hekla is an ideal candidate for constraint of the eruption source parameters (ESPs) used to model tephra dispersal from subplinian–Plinian eruption plumes, including erupted volume, plume height and mass eruption rate (MER). Although several aspects of the more recent, smaller eruptions have been studied in detail (e.g. Gronvold et al. 1983; Gudmundsson et al. 1992; Höskuldsson et al. 2007), ESPs are poorly constrained for the earlier, larger eruptions. More detailed studies of products of these eruptions, and better constraints of the eruptive parameters, are required to fully understand the range in behaviour Hekla exhibits and to permit Hekla to serve as an analogue for other eruptions (e.g. Mastin et al. 2009b).

Most Hekla eruptions prior to 1970 were first studied by Thorarinsson (1967), who mapped the deposits, constructed isopach maps and estimated the eruptive volumes, as well as summarised the contemporary accounts of the eruptive activity. Since then, these events have attracted few interests (e.g. Larsen et al. 1999; Dugmore et al. 2007). Thorarinsson's isopach maps were based on a limited number of thickness measurements, and he did not differentiate between primary thicknesses and reworked material, or distinguish between the deposits of subplinian–Plinian phases and products of later weaker activity. The original volume estimates were calculated using plots of deposit thickness versus average distance of isopachs (Thorarinsson 1954). The resulting 'compressed' volume was then scaled, using estimated volume weights of compressed and uncompressed tephra and taking any reduction in thickness due to compression into account, to the equivalent 'freshly fallen' volume (Thorarinsson 1967). Since Thorarinsson's work there have been significant advances in the field of calculating erupted volume (e.g. Pyle 1989; Fierstein and Nathenson 1992; Bonadonna and Houghton 2005; Bonadonna and Costa 2012; Burden et al. 2013). There is thus merit in revisiting these deposits, in order to better constrain Hekla's eruptive parameters. In this study, we focus on five eruptions between 1104 and 1766, which in terms of total tephra volume erupted are five of the seven largest historical events and thereby a good complement to published data of the more recent, smaller eruptions of Hekla. In addition, these five eruptions were all dispersed to the north, so most of the material was deposited on land, and the deposit footprints partially overlap, which makes it feasible to map them together.

Eruption summaries

The 1104 eruption (also known as the H1 eruption) was the first eruption of Hekla after Iceland was settled. It occurred in the autumn (likely October) of 1104, and although there are no direct written estimates for the duration, the eruption probably lasted for only a few hours to half a day (Thorarinsson 1967). Silicic tephra (initial SiO_2 content of 72 wt%) was deposited over most of Iceland (Thorarinsson 1967; Larsen and Thorarinsson 1977; Larsen et al. 1999). Thorarinsson (1967) originally estimated the tephra volume to be 2.5 km^3 when freshly fallen but later revised it to 2.0 km^3—1.2 km^3 compacted, 0.5 km^3 dense rock equivalent (DRE)—(Larsen and Thorarinsson 1977; Larsen et al. 1999). The H1 eruption is thus the largest historical eruption of Hekla as well as the second largest historical silicic explosive eruption in Iceland, only surpassed by the Öræfajökull eruption in 1362. The eruption caused destruction of several farms (due to 7 to >20 cm of tephra fall). Some of these farms, however, were already close to being abandoned before the eruption started (Thorarinsson 1967).

Following a 54-year repose period, Hekla erupted again on 19 January 1158 (Thorarinsson 1967). As with 1104, there are no constraints on the duration of the eruption but it likely lasted for less than 1 day. Thorarinsson (1967) believed that the eruption was dispersed southward from Hekla but did not map the deposit. Later work by Larsen (1992) determined that the 1158 tephra was deposited northeastward, partially overlapping with the 1104 tephra, and that portions of the distal deposit had erroneously been mapped as part of 1104 by Thorarinsson. The 1158 tephra appears similar to that from 1104 but has slightly lower SiO_2 content (67–68 wt%; Larsen 1992; Larsen et al. 1999) as well as higher FeO and CaO content. Larsen (1992) estimated the tephra volume to be 0.33 km^3 when freshly fallen (0.2 km^3 compacted), covering over 18,000 km^2 on land.

The second largest and the fifth historical eruption of Hekla started on 11 or 12 July 1300 and lasted for 12 months (Thorarinsson 1967). The initial explosive phase was likely short (most likely a few hours and definitely <1 day). A nearly contemporaneous written source describes the opening phase as violent, with darkness from 'sand-fall' lasting a day in northern Iceland. On the second day, darkness was caused by wind remobilising the ash. An estimated 0.5 km^3 of dacitic tephra (0.3 km^3 compacted, 0.125 km^3 DRE) was erupted, of which about 75 % was deposited on land over at least 30,000 km^2 (Thorarinsson 1967; Larsen et al. 1999; Thordarson and Larsen 2007). No definite information was recorded about lava effusion during the eruption, but the 20-

km-long Suðurhraun (or Selsundshraun syðra) lava flow is postulated to have been part of the 1300 eruption. If so, it would be the longest historical lava flow from Hekla. The tephra fall caused destruction of farms and damage to grasslands in northern Iceland, as well as famine in the following year (Thorarinsson 1967).

The eruptions in 1693 and 1766 were both andesitic with approximately 55–60 wt % SiO_2 and each eruption is described by Thorarinsson (1967). The 1693 eruption started in the evening of 13 February and the main, initial phase lasted for about 30 min to 1 h. The eruption started at the summit and then migrated down both flanks along the fissure. The 1693 tephra volume has been estimated as 0.3 km^3 freshly fallen (0.18 km^3 compacted, 0.13 km^3 DRE), of which over 70 % was deposited on land, covering over 22,000 km^2 (e.g. Thorarinsson 1967; Thordarson and Larsen 2007). Weaker activity continued for 7 to 10.5 months, mostly consisting of vulcanian explosions, fountains and multiple lava flows from both ends of the fissure. Over 90 % of the tephra, however, was emitted during the initial phase and deposited northwest of Hekla. A total of 55 farms were damaged or destroyed by less than 1 to about 5 cm of tephra fall, and the ash also caused death of livestock, birds, and fish (Thorarinsson 1967). The 1693 eruption, albeit smaller than the earlier eruptions, was more destructive because its deposits fell farther westward, in a region little affected by previous tephra falls.

The 1766 eruption started in the early morning on 5 April, and the subplinian phase lasted for 5 to 6 h (Thorarinsson 1967). The eruption continued for almost 2 years, including a hiatus between August 1766 and March 1768, ending in April 1768. Most of the later activity consisted of weaker transient explosive events, but there were several more violent explosive phases (most notably on 9 and 21 April and 1 May 1766; and 18 March, 20 April and 7 August 1767) with ash plumes to 4 km. The initial eruption originated from one summit crater and one crater on the SW ridge, after which a fissure along the SW flank and a third crater on the NE flank opened. As many as nine craters are thought to have been active during the entire eruption. Explosive activity was accompanied by lava flows, originating mainly from the SW flank. A total lava volume of about 1.3 km^3 covering 65 km^2 was extruded, making it one of the largest historical flow fields in Iceland. The tephra volume for the eruption has been estimated to be 0.4 km^3 freshly fallen, 0.24 km^3 compacted and 0.18 km^3 DRE (Thorarinsson 1967; Thordarson and Larsen 2007). Over 80 % of the tephra was produced during the initial phase of the eruption, during which the wind direction was toward the north. Although the 1766 eruption was larger than that in 1693, covering over 34,000 km^2 on land, the impacts were much less severe, mainly because the dispersal axis was farther eastward and thereby outside of the main settled area of southern Iceland. Several farms northwest of Hekla were damaged by about 1 cm to less than 5 cm of tephra fall, but these were already subeconomic prior to the eruption. There was also damage to pastures and woodlands, and death of livestock and fish (Thorarinsson 1967).

Stratigraphy

The Hekla tephras form a layered stratigraphy with other fall deposits (Fig. 1), derived mainly from Katla and Bárðarbunga-Veiðivötn in the proximal to medial region, and Katla, Grímsvötn, Bárðarbunga-Veiðivötn and Askja in the distal region, although parts of the stratigraphy may be missing at any site due to syn- and post-eruption erosion. Of particular use for correlations is the c. 871 'Settlement layer' tephras overlying one to three prehistoric black distal falls from Katla, as well as the suite of historical Katla tephras from 934 (Eldgjá), 1500, 1721 and 1918. Marker units such as these are necessary because the preservation potential of the Hekla tephras is surprisingly poor, reflecting exceptionally harsh climatic conditions following, and often during, eruption. Of the 288 new sites visited (Supplementary Table 1), all five of the Hekla tephras are found at only two sites, four at 31 locations, three at 55, two at 82 and one at 118 sites. At single sites, the thickness of any tephra, but particularly the 1104 deposit, can vary by a factor of two to four times reflecting highly localised syn- and post-depositional reworking.

Where only one silicic tephra is present, the 1104 and 1158 deposits can be distinguished only by glass composition. This has led to past miscorrelations and an overestimation of the extent of the 1104 deposit. Of all the historical andesitic Hekla tephras, the 1300 tephra is generally very distinctive due to a high abundance of red lava lithic clasts and the presence of both pumiceous and abundant angular, blocky and scoriaceous juvenile clasts. In the proximal and medial region south and east of Hekla, however, the 1300 tephra cannot be distinguished from the Hekla 1206 tephra in the field. The two can be distinguished by glass composition. The 1693 and 1766 tephras also appear identical in the field and cannot be distinguished if only one is present. Their glass compositions are not sufficiently different to distinguish them. In many locations, they can be identified by their stratigraphic position with respect to the distinctive black ash layer from the 1721 Katla eruption. In the distal region, the andesitic Hekla tephras become darker in colour and are in some locations difficult to differentiate from the Katla ash.

1104 tephra deposit The proximal tephra is up to 1 m thick at 16 km from vent but always partially eroded (Larsen and Thorarinsson 1977). The deposit is generally massive but in places has a finer basal portion. In the eastern sector, the 1104 deposit is often contaminated by a distinct grey fine ash, with higher SiO_2 content, concentrated at several different levels in the lapilli fall deposit.

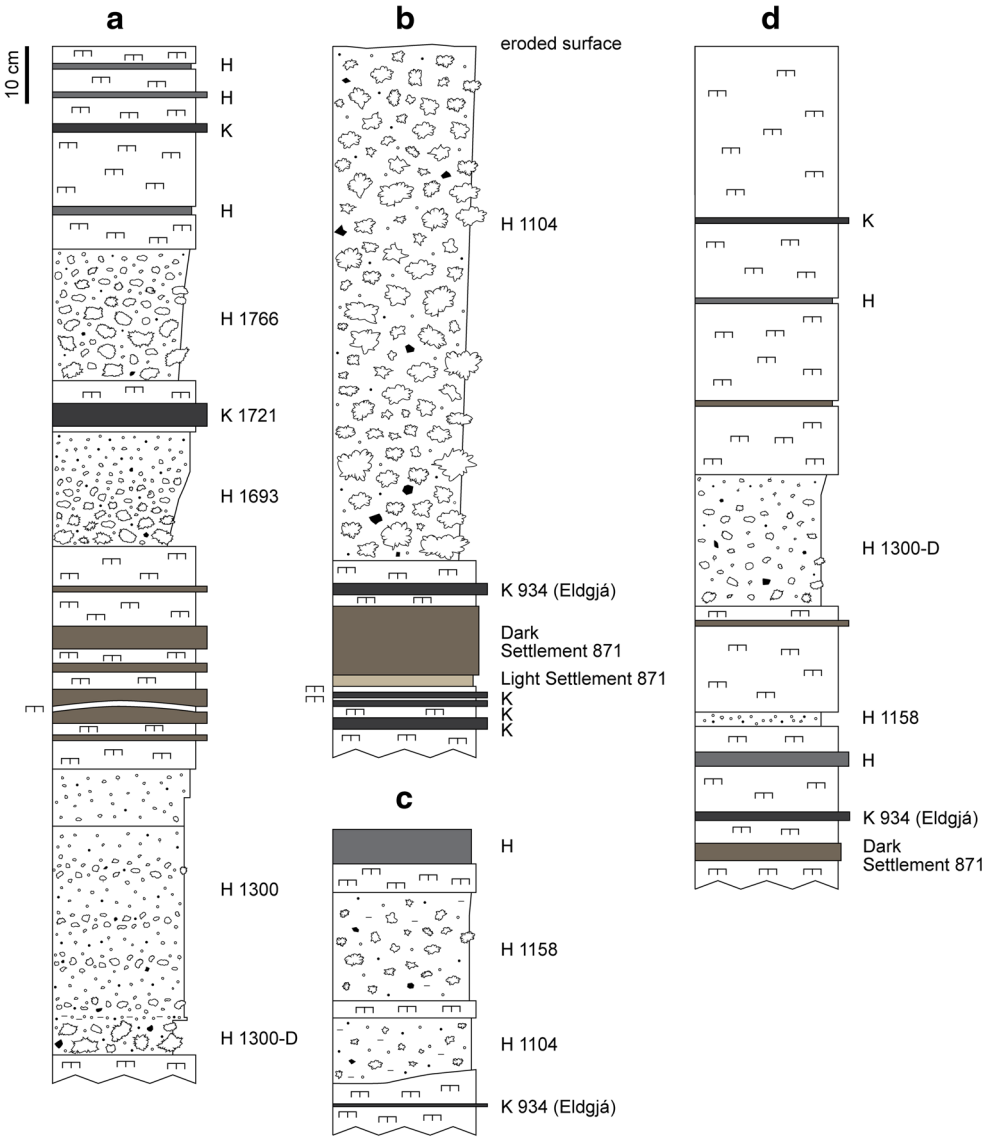

Fig. 1 Stratigraphic logs. Hekla 1104, 1158, 1300, 1693, and 1766 are shown in detail with juvenile clasts in white and wall-rock lithic clasts in *black*. Other historical Hekla tephras are shown as *solid grey*, and ash layers from Katla are shown in *dark grey*. *H* tephras from Hekla, *K* tephras from Katla, "⊓" soil layers. **a**, **b** Logs located 9 km NE of the summit vent of Hekla; **c**, **d** logs located 10 and 47 km NE of the summit vent

1158 tephra deposit The deposit associated with the 1158 eruption reaches a maximum measured thickness of 1.7 m at 5 km from vent and consists of two parts: a lower, coarser and matrix-poor part, and an upper, slightly finer and matrix-bearing part.

1300 tephra deposit In the proximal to medial region, the 1300 deposit consists of multiple subunits. The lowermost unit (herein referred to as 1300-D) is the coarsest and most widely dispersed, and is generally the thickest, corresponding to the initial, most explosive phase of the eruption. Unit D reaches a maximum measured thickness of 26 cm at 10 km from vent. The overlying sequence, which is absent beyond 70 km from vent, consists of a normally graded unit, a massive unit and a finely bedded unit. The dispersal of the upper sequence cannot be mapped in detail, but based on the 34 locations where individual units have been identified, their dispersal is not consistent, and we infer that they resulted from multiple phases of the eruption during which the wind direction shifted.

1693 and 1766 tephra deposits Both deposits associated with the 1693 and 1766 eruptions are massive or weakly normally graded. They reach a maximum measured thickness of 21 and 23 cm respectively at 9 km from vent.

Methodology

New isopach maps were constructed combining the data from Thorarinsson (1967) and Larsen (1992) with new thickness measurements at 288 locations across Iceland and previously unpublished data (from Larsen, unpublished data 2016). For the eruption in 1158, the isopach

Table 1 Overview of exponential segments fits for the 1104, 1158, 1300, 1300-D, 1693, and 1766 Hekla eruptions

Eruption	Map version[a]	Exp segments	R^2 values	*BS* (km)	B_T (km)
1104	MAP-1	2	0.990, 1	96	13, 26
	MAP-2	3	0.946, 1, 0.994	16, 61	2, 8, 28
1158	MAP-1	2	0.994, 1	45	4, 23
	MAP-2	3	1, 0.994, 1	10, 46	1, 4, 30
1300	MAP-1	2	0.967, 1	44	7, 22
	MAP-2	2	0.988, 0.982	31	5, 16
1300-D	MAP-2	2	0.988, 0.970	32	6, 20
1693	MAP-1	2	1, 1	26	4, 20
	MAP-2	2	0.999, 0.991	36	4, 17
1766	MAP-1	2	1, 1	33	5, 26
	MAP-2	2	1, 0.994	39	4, 24

BS break-in-slope distance from vent of individual exponential segments, B_T thinning half distance on semi-log plots of thickness versus square root of isopach area of each segments

[a] MAP-1 uses the original thickness-area estimates by Thorarinsson (1967). MAP-2 is the new isopach map (Fig. 2). For Hekla 1158, MAP-1 is the isopach map by Larsen (1992) and MAP-2 is the revised map with one additional proximal isopach line

map by Larsen (1992) was revised with the addition of one proximal isopach line. Two new maps were produced for the eruption in 1300: one for the total thickness of the deposit and one for unit D only. Due to the poor preservation, especially for the distal products, an alternative set of isopach maps for the eruptions in 1104, 1300, 1300-D, 1693, and 1766, was constructed using historical information recorded in Thorarinsson (1967), and the results for these are discussed in supplementary document 1. The only difference between the two sets is in how the outermost isopach line is defined.

Eruptive volumes were calculated by integrating best-fit lines on semi-log plots of thickness versus square root of isopach area, using three different approaches: exponential (Pyle 1989; Fierstein and Nathenson 1992), the power - law (Bonadonna and Houghton 2005) and the Weibull function (Bonadonna and Costa 2012). The number of exponential segments used and the associated break-in-slope (*BS*) distances and thinning half distances (B_T) are reported in Table 1. Both the exponential and the Weibull function were integrated from zero to infinity, but the power-law requires the identification of integration limits. For all the eruptions, the power-law exponent (k) is <2 (see Table 2), and, therefore, the volume strongly depends on the outer integration limit (i.e. the distal extrapolation) but is not sensitive to the inner integration limit (Bonadonna and Costa 2012). The inner integration limit was set to a fixed value determined following Bonadonna and Houghton (2005). The outer integration limit, for which no set protocol exists, was set as the area

Table 2 Overview of power-law fits for the 1104, 1158, 1300, 1300-D, 1693, and 1766 Hekla eruptions

Eruption	Map version[a]	PL exponent[b]	R^2 value	Integration limit[c] (km)
1104	MAP-1	1.623	0.906	406
	MAP-2	1.768	0.985	455
1158	MAP-1	2.040	0.971	357
	MAP-2	2.016	0.982	357
1300	MAP-1	1.461	0.976	339
	MAP-2	1.884	0.971	289
1300-D	MAP-2	1.428	0.940	322
1693	MAP-1	1.464	0.999	296
	MAP-2	1.969	0.984	250
1766	MAP-1	1.484	0.994	387
	MAP-2	1.966	0.985	331

[a] MAP-1 is the original thickness-area estimates by Thorarinsson (1967). MAP-2 is the new isopach map (Fig. 2). For Hekla 1158, MAP-1 is the isopach map by Larsen (1992) and MAP-2 is the revised map with one additional proximal isopach line

[b] k from $T = T_o\,(A^{1/2})^{-k}$

[c] Value determined from where the last exponential segment reach a thickness equal to 0.01 cm

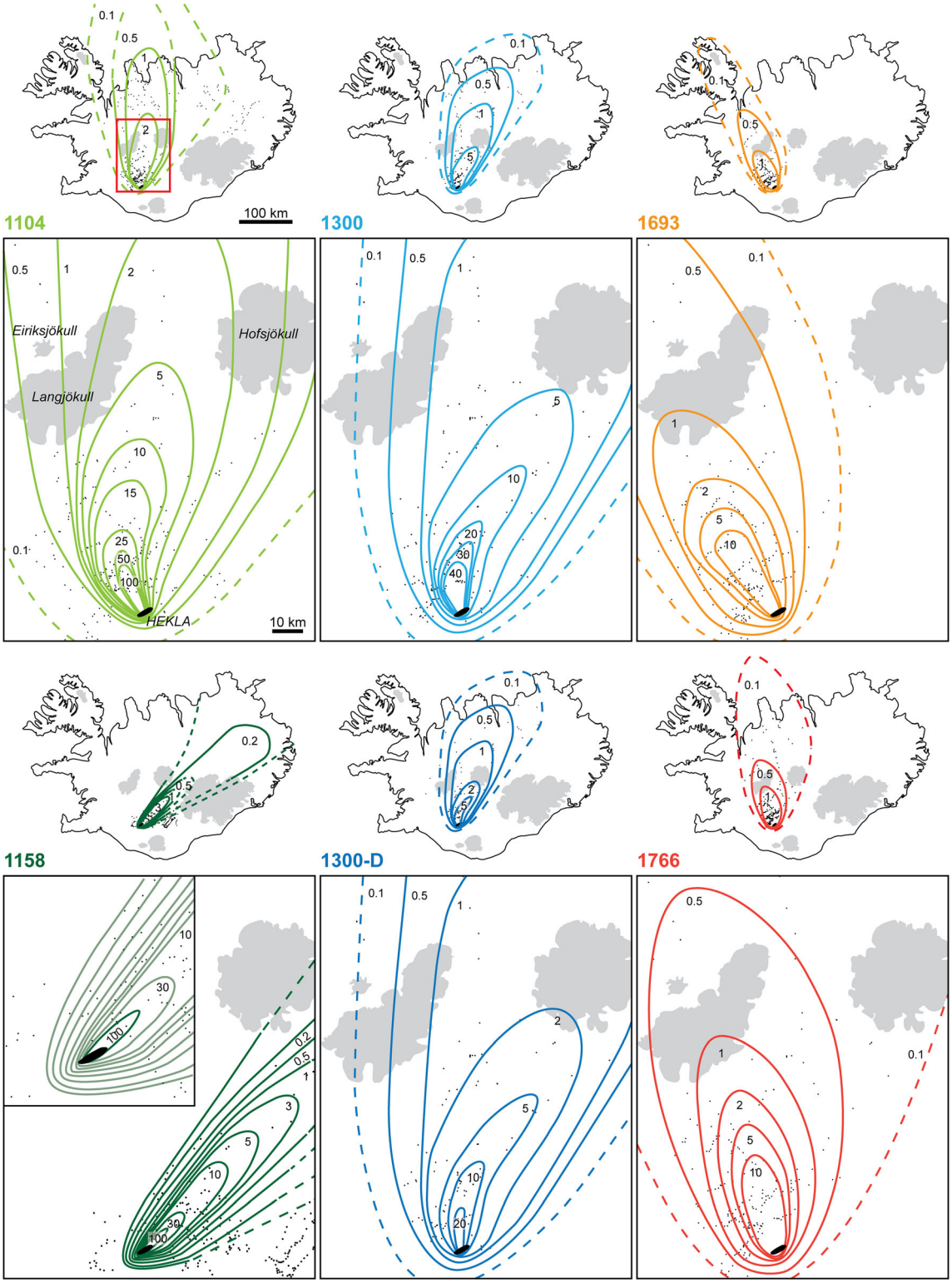

Fig. 2 New isopach maps for Hekla 1104, 1158, 1300, 1300-D, 1693, and 1766. All isopach labels (values in cm) are located on the inside of the corresponding isopach line. The *dashed line* is the outermost mapped isopach line (0.1 cm). The *red box* in the 1104 map shows the close-up area for all eruptions. The 1158 isopach map is modified from Larsen (1992) with the addition of one more proximal isopach line. Glaciers are shown in *grey*. Coordinates of measured sections are listed in Supplementary Table 1

for which the last exponential segment reaches a thickness of 0.1 mm ± 20 % of that area (see Table 2). Alternative outer limits, such as 0.1, 0.01 and 0.001 % of the maximum thickness obtained by the exponential segments

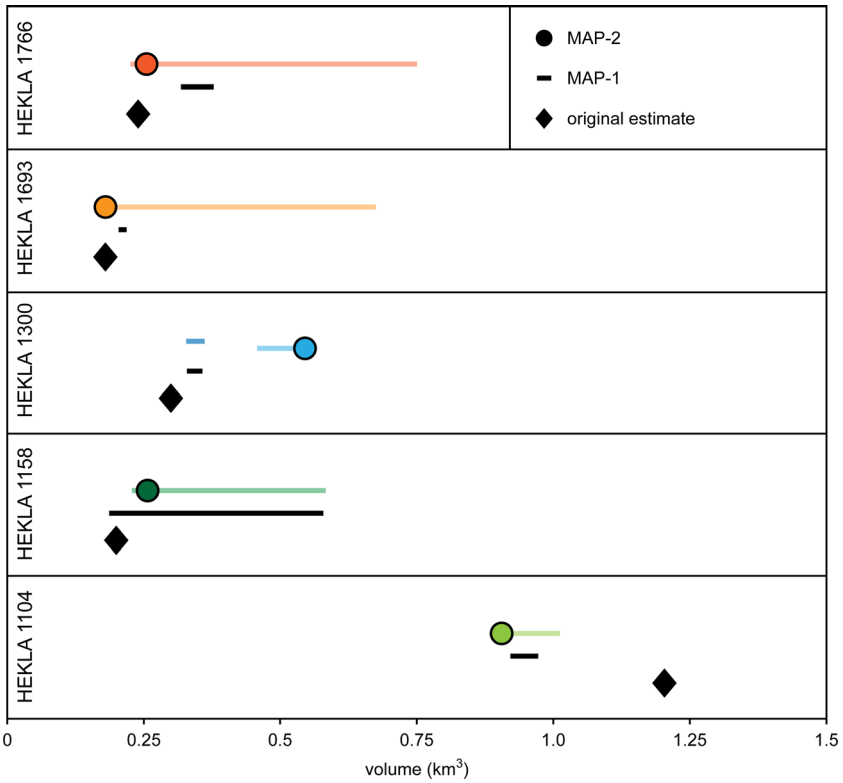

Fig. 3 Overview of the new volume results for Hekla 1104, 1158, 1300, 1693, and 1766. The original estimates are shown in *black diamonds*, and the *black bar* shows the range in volume obtained for the original thickness-area estimates (*MAP-1*) using the exponential segments, power - law, and Weibull function. *Coloured circles* correspond to the result with exponential segments for the revised isopach map (Fig. 2, *MAP-2*). The *coloured bar* shows the range in volume obtained for each map when including the power-law and Weibull function. For Hekla 1300, the *darker bar* shows the volume range for unit 1300-D

(Klawonn et al. 2014b; personal communication), were also tested.

The volumes for these eruptions were also calculated using Thorarinsson's (1967) original thickness-area estimates (i.e. MAP-1), in order to distinguish between changes in volume caused by the difference in method applied in this study and the previous estimates. Two sets of volumes were also calculated for the deposit generated by the 1158 eruption; one set using only the original isopach map (MAP-1) for which Larsen (1992) estimated the volume from a plot of area versus thickness using an assumed maximum thickness of 2 m, and one set using the revised isopach map (MAP-2) which has one additional proximal isopach line. For all the eruptions, the volume contribution from the part of the deposit that is well constrained by the isopach lines versus the distal and proximal contribution (i.e. the part of the volume caused by extrapolating the best-fit curve beyond the isopach lines) was determined following Klawonn et al. (2014b). The cut-off between the proximal and well-defined portion equalled the most proximal isopach line of each map. In order to be able to compare the effect of the outermost isopach line, the cutoff between the well-defined portion and distal was set to the 0.5-cm isopach line, rather than the outermost isopach line as by Klawonn et al. (2014b).

Isopleth maps were constructed for 1104, 1300-D, 1693, and 1766. The maximum lithic clast size (ML) was determined at sample sites by taking the average of the three principal axes of the five largest clasts. Plume heights and wind speeds were estimated following Carey and Sparks (1986) using a lithic clast density of 2500 kg m^{-3}. Alternative plume heights were calculated from the volume estimates (Mastin et al. 2009b) using the correlation

$$H = 25.9 + 6.64\log_{10}(V)$$

where H is the plume height in kilometres and V is the total DRE volume in cubic kilometres. An average deposit density of 500 kg m^{-3} and a DRE value of 2500 kg m^{-3} were used to convert from volume to DRE volume. Time-averaged MERs were derived from the plume heights using the approaches by Wilson and Walker (1987) and Mastin et al. (2009b). MERs were also calculated using the method of Degruyter and Bonadonna (2012). For the latter, both eruption temperature and plume height, and the associated wind speed, were varied, whereas the radial entrainment and wind entrainment coefficients were set to 0.1 and 0.5, respectively (Degruyter and Bonadonna 2012; Bonadonna et al. 2015b). Temperature was varied in the range 923–1273 K according to magma composition, whereas plume height and wind speed were derived from the model of Carey and Sparks (1986). In particular, wind speed was calculated at the tropopause and averaged along the plume rise height assuming a linear decrease from tropopause to sea level and a linear increase from tropopause to the top of stratosphere (Carey and Sparks 1986; Bonadonna and Phillips 2003; Degruyter and Bonadonna 2012). The scaling parameter Π was also derived from the method of

Degruyter and Bonadonna (2012) to infer insights into plume dynamics.

Results

Additional proximal isopach lines have been added to the 1104, 1158, and 1300 maps, increasing the most proximal isopach to 1 m for 1104 and 1158, and 40 cm for 1300 compared with 20, 30, and 20 cm, respectively, for the original maps (Fig. 2). The crosswind and downwind extents of the majority of the other isopach lines have been modified. Based on the revised isopach maps, the dispersal axes for both the 1104 and 1300 tephras are farther east than originally described (Thorarinsson 1967).

Figure 3 and Table 3 show a summary of the new volume estimates for the range of methods used. For 1158, 1300, 1693, and 1766, the new volume estimates are equal to or larger (depending on method used) than the original estimates by Thorarinsson (1967) and Larsen (1992). For 1104, the revised isopach map yields a smaller volume than the original estimate, independent on method used. Thorarinsson's (1967) original thickness estimates (MAP-1) yield slightly larger volumes using the current methods of integration, compared with his original estimates, for all eruptions except 1104. The volume increases for the new isopach maps compared with the original estimates cannot be attributed only to the change in volume calculation method. The new volumes, independent of method used, however, do not change the VEI assignment for any of the eruptions. Figure 4 shows the volume for each eruption partitioned into the part of the deposit that is well constrained by the isopach maps (here defined as the area between the most proximal isopach line and the 0.5-cm isopach line) and the less well-constrained distal and proximal contributions for each eruption (cf. Klawonn et al. 2014b). For each eruption, the three methods give similar volumes for the well-constrained portion but differ significantly in their estimates of both the proximal and distal volumes.

Isopleth maps for the 1104, 1300-D, 1693, and 1766 deposits are shown in Fig. 5. Based on these maps (Carey and Sparks 1986), the plume height is inferred to have been approximately 20–25 km for 1104, 21–25 km for 1300-D, 13–17 km for 1693 and 17–18 km for 1766 (see Table 4). The volume-derived plume height (Mastin et al. 2009b) for the 1158 eruption is 17–20 km. The estimated plume heights correspond to MERs of 5.3×10^7 to 1.2×10^8 kg s^{-1} for 1104, 2.7×10^7 to 4.8×10^7 kg s^{-1} for 1158, 6.9×10^7 to 1.2×10^8 kg s^{-1} for 1300-D, 9.2×10^6 to 3.2×10^7 kg s^{-1} for 1693 and 3.0×10^7 to 3.2×10^7 kg s^{-1} for 1766, calculated with the method of Wilson and Walker (1987). Including the effect of wind and eruption temperature (Degruyter and Bonadonna 2012), yields MERs that are about four to eight times larger than the time-averaged MERs (see Fig. 6). The scaling parameter Π, which is a way to quantify the effect of wind on plume rise, is in the range of 0.2 to 0.4 for all four eruptions, typical of transitional plumes (Degruyter and Bonadonna 2012; Bonadonna et al. 2015b). For comparison, the plume heights, and corresponding MERs, derived from volumes (Mastin et al. 2009b) are listed in Supplementary Table 5. The volume-derived plume heights are generally comparable with or slightly lower than those determined using Carey and Sparks (1986).

Based on the dispersal, all five eruptions are Plinian according to the classification scheme by Walker (1973). Using the simplified classification scheme by Bonadonna and Costa (2013), which is based on plume height and intensity, the 1158, 1693 and 1766 eruptions are subplinian, whereas the 1104 and 1300-D eruptions are

Table 3 Overview of new volume results in km^3 for the 1104, 1158, 1300, 1300-D, 1693, and 1766 Hekla eruptions, using the three main integration fits (exponential segments, power -law and Weibull function)

Method	Hekla 1104		Hekla 1158		Hekla 1300		Hekla 1300-D	Hekla 1693		Hekla 1766	
	MAP-1	MAP-2	MAP-1	MAP-2	MAP-1	MAP-2	MAP-2	MAP-1	MAP-2	MAP-1	MAP-2
Exponential segments[a]	0.93	*0.91*	0.19	*0.26*	0.34	0.55	0.35	0.21	0.18	0.33	0.26
Power-law[b]	0.97	0.92	0.19	0.23	0.35	0.46	0.36	0.21	0.18	0.32	0.23
Weibull function[c]	0.93	1.01	0.57	0.58	0.33	0.56	0.33	0.21	0.67	0.37	0.75

MAP-1 is the original thickness-area estimates by Thorarinsson (1967); MAP-2 is the new isopach map (Fig. 2). For Hekla 1158, MAP-1 is the isopach map by Larsen (1992) and MAP-2 is the revised map with one additional proximal isopach line. Full comparison of volume estimates using variations of each method is shown in Supplementary Table 7, and the change in power-law volume when varying the outer integration limit by ± 20 % is shown in Supplementary Table 6

[a] Using the equation from Bonadonna and Houghton (2005). Two exponential segments were used for all maps, except the ones set in italics, for which three segments were used

[b] Average volume from proximal limit calculated following Bonadonna and Houghton (2005), distal limit calculated from distal exponential segment equal to 0.1 mm ± 20 %. For all maps, except 1158, the power-law exponent (k) has a value <2

[c] Using the spreadsheet by Bonadonna and Costa (2012) and free parameter limits by Bonadonna and Costa (2013)

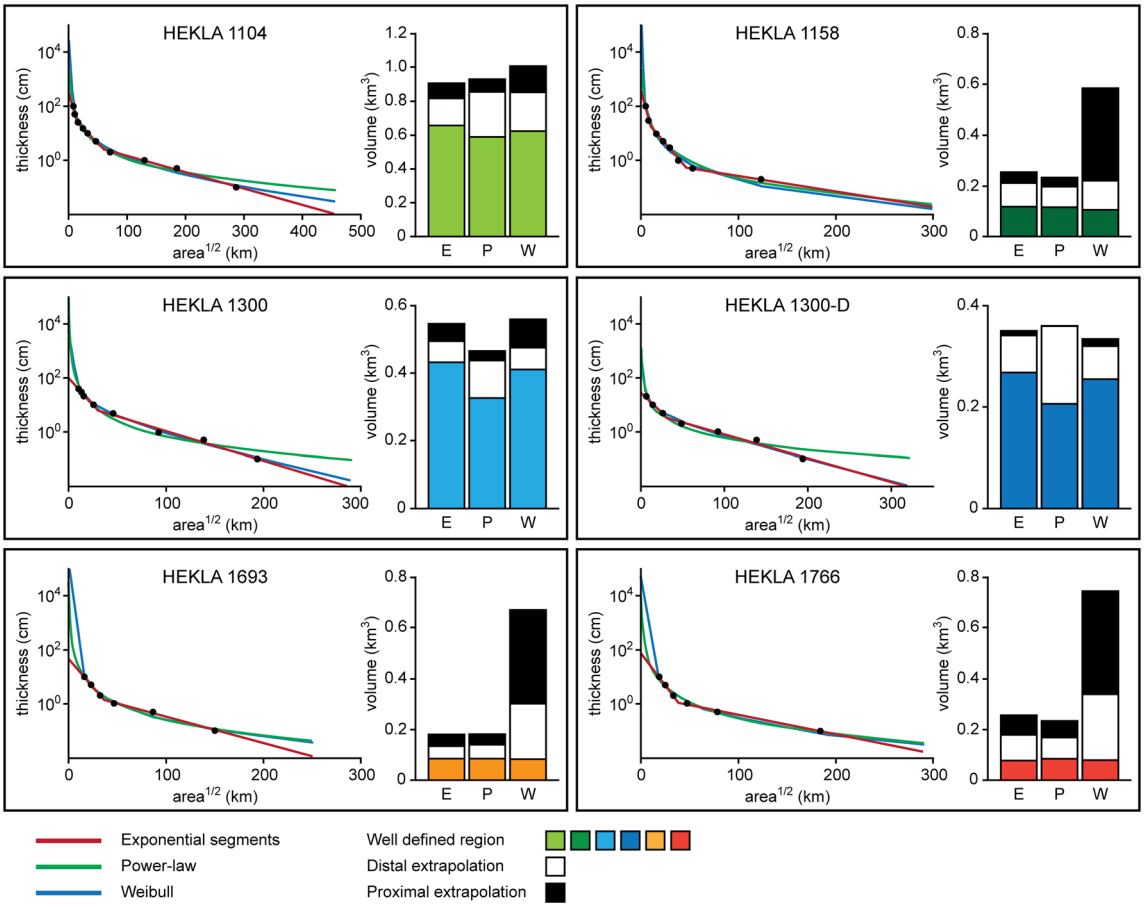

Fig. 4 Thickness-square root of area semi-log plots for the new isopach maps (Fig. 2) for Hekla 1104, 1158, 1300, 1300-D, 1693, and 1766. The best fit for exponential segments is shown in *red*, power -law in *green* and Weibull function in *blue*. For the 1158, 1693, and 1766 eruptions, the Weibull function converges with the power-law curve. The insets show the resulting volume for each method. For each eruption, the volume portion resulting from the region well constrained by the isopach maps is shown in colour, the volume portion resulting from the distal extrapolation is shown in *white*, and the volume portion resulting from the proximal extrapolation is shown in *black*

subplinian–Plinian, when using the MER estimated following Wilson and Walker (1987). Use of the MER following Degruyter and Bonadonna (2012) classifies the 1693 and 1766 eruptions as subplinian–Plinian and the 1104 and 1300-D eruptions as Plinian.

Discussion

Variability in bulk volume estimates with method used

The issues with estimating volumes of pyroclastic deposits, and the associated uncertainties, have been discussed in detail in multiple studies (e.g. Bonadonna and Houghton 2005; Carey et al. 2009; Bonadonna and Costa 2012; Le Pennec et al. 2012; Biass et al. 2014a; Klawonn et al. 2014a, b; Bonadonna et al. 2015a). Estimated volumes are dependent on the algorithm used, and more importantly, on how well constrained the deposit is, especially in the proximal and distal fields (e.g. Klawonn et al. 2014b). The new Hekla results highlight both of these issues.

The exponential technique results in either the smallest or intermediate volume estimate for all the studied eruptions. Where it yields the intermediate volume estimate, it is generally closer to the minimum estimate than to the maximum. Previous studies (e.g. Bonadonna et al. 1998; Bonadonna and Houghton 2005) have shown that the use of exponential fitting may underestimate the volume unless at least three segments are identified, corresponding to the three sedimentation regimes (turbulent, intermediate, laminar) associated with the umbrella cloud spreading.

The power-law relationship yields volumes that range from 15 % smaller to 2 % larger than the volumes derived from the exponential segments. In most cases, however, the volume difference between the two methods is less than 10 %. The worst agreements occur where the power-law function has a poor fit to the most distal data point. The effect increases in magnitude with a wider

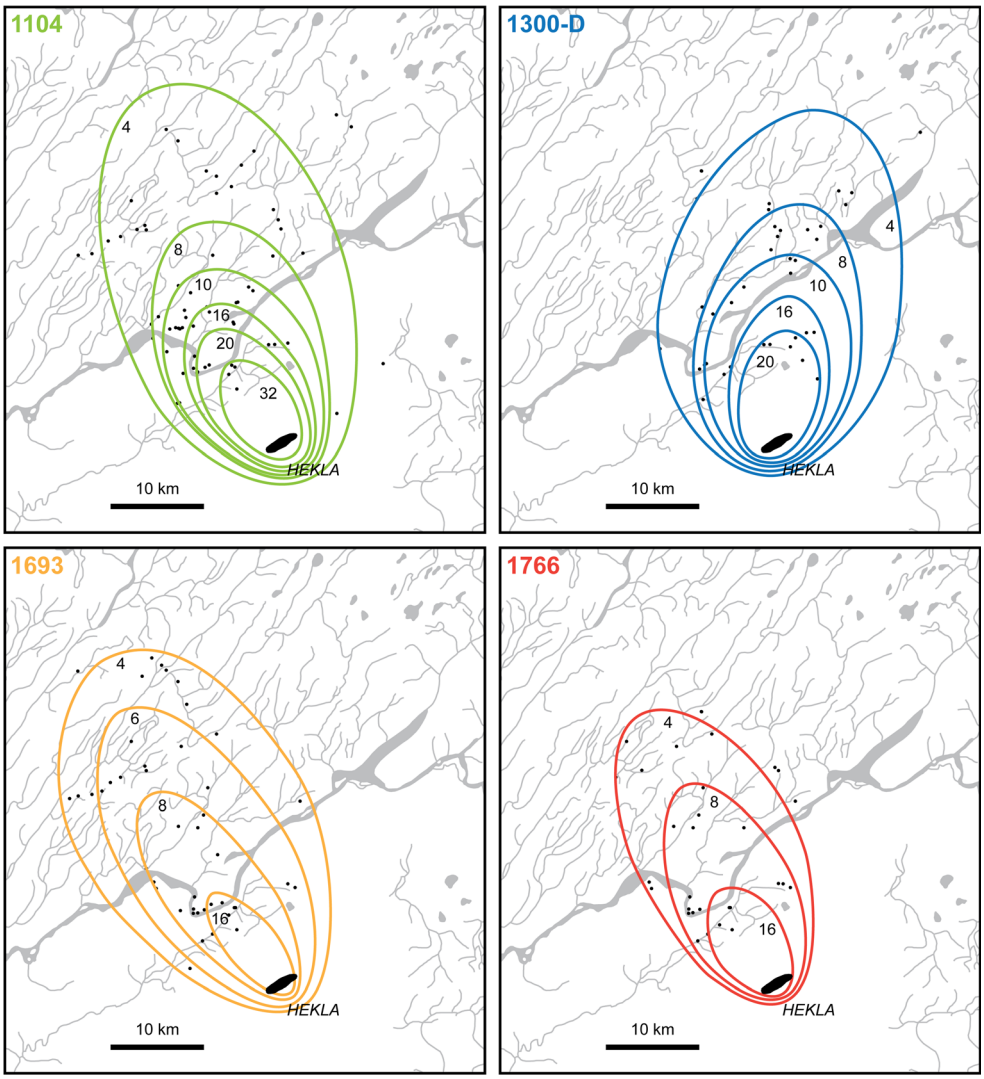

Fig. 5 Isopleth maps for the Hekla 1104, 1300-D, 1693, and 1766 eruptions. All isopleth labels (values in mm) are located on the inside of the corresponding isopleth line. North is to the top of the figure. Lakes, rivers and streams are shown in *grey*. Locations where maximum lithic clast size was measured are shown as *black dots*

Table 4 New eruptive parameters for selected Hekla eruptions

Eruption	VEI[a]	Volume[b] (km^3)	Plume height[c] (km)	Wind speed[c] ($m\ s^{-1}$)	Mass eruption rate[d] ($kg\ s^{-1}$)
1104	4–5	0.9–1.0	20.1–24.5	30	5.3×10^7–1.2×10^8
1158	4	0.2–0.6	17.0–19.7		2.7×10^7–4.8×10^7
1300	4	0.5–0.6			
1300-D	4	0.3–0.4	21.5–24.7	30	6.9×10^7–1.2×10^8
1693	4	0.2–0.7	13.0–17.7	30–32	9.2×10^6–3.2×10^7
1766	4	0.2–0.8	17.5–17.8	30–32	3.0×10^7–3.2×10^7

[a] Following Houghton et al. (2013)

[b] Range of volumes obtained from isopach maps in Fig. 2, using two or three exponential segments, average of power-law integrated to 0.1 mm thickness ±20 % from last exponential segment and Weibull function with free parameter limits by Bonadonna and Costa (2013)

[c] Following Carey and Sparks (1986) for all except the 1158 eruption, for which Mastin et al. (2009b) was used. The 32, 16 and 8 mm isopleths were used for the 1104 eruption, and 16 and 8 mm isopleths were used for the 1300-D, 1693 and 1766 eruptions

[d] Following Wilson and Walker (1987), see Fig. 6 for MERs determined following Degruyter and Bonadonna (2012)

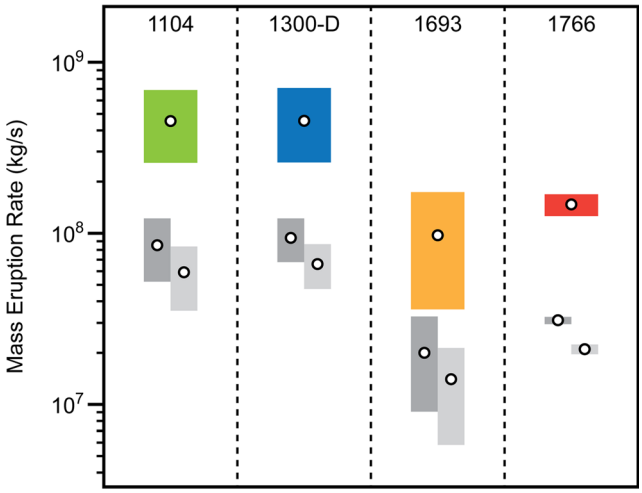

Fig. 6 Comparison of mass eruption rate determined for selected Hekla eruptions using three different methods. The *circles* correspond to the average MER by each method. The *coloured bars* show the range in MER using Degruyter and Bonadonna (2012), *dark grey* is the range using Wilson and Walker (1987) and *light grey* is the range in MER using Mastin et al. (2009b). Plume heights used for all eruptions were determined following Carey and Sparks (1986) using the isopleths in Fig. 5. For Degruyter and Bonadonna (2012), both temperature and plume height, and associated wind speed, were varied

outer limit. One of the main issues with applying a power law is that when the power-law exponent is <2, it might result in unrealistically large volumes due to difficulties in assigning an appropriate outer limit (Bonadonna and Houghton 2005). A value of power-law exponent <2 is typical of the gradual thinning of large subplinian/Plinian eruptions but can also be associated with small to moderate eruptions with poor deposit exposure. For comparative purposes in this study, we use data from the distal exponential segment to constrain the outer limit for the power-law calculation; the data yield a reasonable, although conservative, estimate for the outer limit. By comparison, use of 0.1 % of the maximum thickness (T_o) obtained from the first exponential segment as the outer limit results in a larger difference between the volume derived by the two methods (range from 22 % smaller to 83 % larger).

For all of the revised isopach maps, except for that of the 1300-D eruption, the Weibull function results in the largest volume, from 102 to 372 % of the volume derived from the exponential segments. One advantage of the Weibull function is that with three free parameters it can be modified to fit a range of thinning conditions. It tends to converge with the exponential segments if the thinning is constrained by few data points and with the power-law function if the thinning is constrained by many data points. Limitations of the Weibull function are that it cannot be used with less than four isopach lines, and the resulting best-fit solution is very sensitive to the most distal isopach, which also is the hardest to constrain (Bonadonna and Costa 2013). For example, for these Hekla eruptions, artificially excluding the most distal isopach line results in a >20 % volume increase for two of the maps and >50 % decrease for one of the maps.

Influence of data quality and availability on volume estimates

For many deposits, the proximal and the distal regions are the most difficult to constrain. The proximal outcrops are not always accessible due to burial or destruction by subsequent eruptions, whereas the distal deposit might be extensively eroded or lacking if, for example, deposited over water. For these Hekla eruptions, the most proximal region has been buried by lava flows. For the distal region, the preservation potential, even during the eruptions, was low and part of the distal tephra fall also occurred over the ocean. The difference in volume obtained by changing the outermost isopach line is further discussed in Supplementary document 1.

A more insightful approach to comparing and evaluating the volume results is in terms of relative volume contributions from the part of the deposit that is well constrained by the distribution of sample points, versus the poorly constrained proximal and distal portions (regions A, C and B respectively in Klawonn et al. 2014b) shown in Fig. 4. The definition of these three portions is dependent on the sample point distribution. Even for these Hekla eruptions, the length of the proximal and well-constrained region along the dispersal axis varies significantly (see Table 5). The well-constrained region corresponds to downwind distances from about 15–20 km from vent to 200–400 km from vent for the eruptions in 1104, 1158, and 1300, whereas for the eruptions in 1693 and 1766, the equivalent region extends only 35–165 and 35–120 km downwind from vent, respectively.

The observed differences in volume, obtained from the different methods, are in the poorly constrained proximal and distal volumes. For the 1104, 1300 and 1300-D deposits, the power - law yields a slightly larger distal volume than the exponential segments. For the eruptions where the Weibull

Table 5 Length downwind along dispersal axis of proximal vs constrained region

Eruption	Proximal (km)	Well constrained[a] (km)
1104	17	358 (17–375)
1158	13	267 (13–230)
1300	20	210 (20–230)
1300-D	15	215 (15–230)
1693	35	130 (35–165)
1766	35	85 (35–120)

[a] Defined as the region from the most proximal isopach line to the 0.5-cm isopach line

function gives the largest volume, a volume increase is associated with the distal portion, but there is also a large proximal contribution for some of the eruptions. For the 1158, 1693 and 1766 deposits, the Weibull proximal volume constitutes 55–62 % of the total volume. The large proximal volume results from the Weibull function converging with the power-law function for these eruptions and thereby approaching infinity at the inner integration limit. For both the 1693 and 1766 deposits, the well-constrained part of the deposit amounts to <12 % of the total Weibull volume versus <50 % when using the exponential segments and power-law fit. The fact that such significant volumes lie beyond the well-constrained part of the deposit means that large uncertainties still remain regarding the true volumes of these eruptions. As pointed out by Klawonn et al. (2014b), more care is required when comparing volumes, and it is better to report both the well-constrained volume and the extrapolated total volume.

Hekla eruption source parameters

As already shown for other deposits (e.g. Bonadonna and Costa 2012; Bonadonna et al. 2015a), the erupted volume strongly depends on the selected best-fit function (i.e. exponential, power-law, Weibull). This is true also for the case of the studied Hekla eruptions (e.g. Fig. 4). Uncertainties in the determination of critical ESPs, such as the erupted volume, have important implications for real-time forecasting of new eruptions and hazard assessment. As with the eruptions cited in Klawonn et al. (2014b), these Hekla data show good agreement for only the regions that are well constrained by the distribution of sample points.

We consider exponential fitting to be a reliable strategy to provide a minimum volume estimate (e.g. Pyle 1989, 1995; Bonadonna and Houghton 2005). For the 1104 and 1158 deposits, the thinning rate was best described by three segments, with thinning half distances (B_T) of <4, 4–10 and >20 km for the three segments (see Table 1). Predictably, the 1104 deposit thins more gradually than the 1158 deposit. The first break-in-slope (*BS*) occurs at 16 and 10 km from vent for the 1104 and 1158 deposits, respectively. The other three deposits are not well constrained between the source and 15–32 km, with the first apparent *BS* occurring >30 km from vent (Table 1). These *BS* values are likely associated with the poor deposit exposure than to real shifts in sedimentation regimes. The thinning trends for the 1300-D, 1693, and 1766 deposits are defined by only two segments. In theory, thinning should be best described by a minimum of three segments, thought to correspond to different sedimentation regimes for clasts being deposited (Bonadonna et al. 1998). For each of these eruptions, the equivalents of segment SEG0 of Bonadonna et al. (1998) (i.e. segment associated with plume-margin fallout) are not described as the most proximal isopach line is only 10 or 20 cm. In fact, the first *BS* for a 25- and 17-km plume height should be around 9 and 5 km, respectively (Bonadonna and Phillips 2003), while all observed *BS* are at distances of >11 km. It is likely that more proximal isopach data would have helped define additional more steeply sloping segments. This proved to be the case for the new data for the 1158 deposit, where the addition of one more proximal isopach line in the new version of the isopach map resulted in an additional segment and a corresponding shift of the first break-in-slope point to 10 km from the original 45 km.

We find that using the last exponential segment to constrain the outer integration limit for the power-law function is a good compromise for these five eruptions. In the case of these deposits, modifying this outer integration limit by ± 20 % results in a volume change of 4–14 % (see Supplementary Table 6) and the average of the minimum and maximum volume is a good estimate of the power-law volume. We prefer this approach rather than using a percentage of the maximum thickness obtained from the first exponential segment (cf. Klawonn et al. 2014b) because, for these eruptions, the latter approach yields unrealistically large deposit areas with commensurately unrealistically large deposit volumes (see Supplementary Table 7).

The Weibull function could potentially be very useful for calculating deposit volumes due to its ability to reproduce the gradual thinning of tephra deposits and to allow for the integration between zero and infinity that represent a good compromise between the exponential and the power-law strategies. The application of the Weibull fitting to the 1158, 1693, and 1766 deposits, however, results in a significantly larger volume than the other two methods. In these cases, the Weibull function converges with the power-law in the distal region. As expected, it therefore yields a larger distal volume than do the exponential segment fits. Due to the difference in integration limits, it also results in a larger distal volume than the power-law fits. More importantly, the Weibull function yields a proximal volume that is five to eight times larger than those from the other functions. Consequently, 80–90 % of the total volume comes from extrapolating beyond the area of the mapped deposit. Clearly, the application of the Weibull fitting to these Hekla deposits is strongly sensitive to the lack of proximal data.

Considering the wide range of volumes associated with these Hekla eruptions, mostly due to poor deposit exposure (Fig. 3; Table 3), a reliable volume estimate cannot be derived. Only a minimum estimate based on the integration of two or three exponential segments can be provided, which is associated with the well-constrained portion of the deposit. Our results, therefore, highlight how deposit exposure is more important than the choice of integration method for obtaining accurate volume estimates. In addition, only a minimum estimate of erupted volume can be safely provided when large parts of the deposits are not accessible or missing (as for these Hekla deposits). Care needs to be taken to minimise the

proportion of the total volume arising from extrapolating beyond the isopach maps.

Both the 1104 and 1300/1300-D deposits (Fig. 2) have a bend in the dispersal axes. A common explanation for this is that the wind field changed with time during the course of the eruption (i.e. rotated toward the east during these two eruptions) or that the wind field changed with elevation. Although no specific constraints on the duration for these older Hekla eruptions exist, they were probably similar to the other Hekla eruptions, lasting only one to a few hours. It is thus not likely that these bends represent an easterly shift in the wind direction with time.

The dispersal bend occurs for the two largest eruptions with the two largest volumes and highest plumes. For the 1104 deposit, the bend occurs between the 50- and 25-cm isopach lines, about 25–30 km downwind. For the 1300-D deposit, the bend is less pronounced, occurring between the 20- and 10-cm isopach lines about 15–30 km downwind. The bend occurs both for the 1300 and 1300-D deposits, so it is not caused solely by the 1300 map being a composite of multiple eruptive phases for which the wind direction was different.

We interpret this bend, both for the 1104 and 1300-D deposits, to result from parts of the plume interacting with winds of different direction and speed at different altitudes, similar to what was observed during the Grímsvötn eruption in 2011 (Gudmundsson et al. 2012). During this eruption, the plume spread laterally simultaneously at two altitudes (see e.g. Fig. 4 in Petersen et al. 2012); a more ash-rich plume in the mid-troposphere and a less ash-rich (more SO_2 gas rich) plume in the upper troposphere–lower stratosphere (Cooke et al. 2014).

Implications for source terms used in tephra-dispersal forecasting

To determine eruptive parameters accurately, it is important both to thoroughly characterise eruptions for use as ESPs in models for real-time forecasting (e.g. by the Volcanic Ash Advisory Centres (VAACs)) and long-term hazard assessments (e.g. Cioni et al. 2003; Folch and Sulpizio 2010; Jenkins et al. 2012). Mastin et al. (2009b) highlighted the issues associated with assigning ESPs for ongoing eruptions. Their attempt to revise ESP relationships, specifically the relationship of eruptive volume, plume height and MER is a good first-order solution by which historical eruptions are used as a template to assign ESPs. For Mastin et al. (2009b), volume of previous eruptions is the most important parameter to constrain accurately, since they use this to derive plume height and thus MER. Although not discussed in this paper, the volume (as a proxy for eruption magnitude) is also used to assign an arbitrary mass proportion of fine material (e.g. Mastin et al. 2009b; Beckett et al. 2015).

The five Hekla eruptions herein highlight the problems associated with determining tephra volume for eruptions with poorly preserved deposits, such as those that fall over oceans, glaciers or in areas where erosion rate is higher than soil accumulation, with extensive reworking and/or removal of the tephra. The difficulty in characterising precisely both the proximal and distal portions of the deposit, and hence calculating volume, leads to further consequential uncertainties in other ESPs, mainly plume height and MER. For these Hekla eruptions, estimates of plume height using the approach of Mastin et al. (2009b) are fairly insensitive to changes in calculated volumes. The volume-derived plume heights (see Supplementary Table 5) are generally within 3 km of those determined from isopleth maps. The range in volume from the different integration methods generally leads to less than 0.5 km variation in plume height, corresponding to a difference in MER of up to 10^7 kg s^{-1}. The exception is those eruptions where the Weibull function resulted in a significantly larger volume, corresponding to an up to 4 km higher plume and consequently up to 3×10^7 kg s^{-1} larger MER.

The discrepancies between plume heights derived from the isopleths and the volume-derived plume heights are expected. The correlation by Mastin et al. (2009b) shows a 20 % typical error in volume-derived plume height. An earlier compilation by Carey and Sigurdsson (1989) investigating the relationship between plume height and erupted mass for Plinian eruptions showed similar scatter. One of the limitations of deriving plume heights from volume is that duration is not accounted for (Mastin et al. 2009b). A larger volume is assumed to result from a higher plume, but a large volume could also result from a lower plume of longer duration. This approach thus yields a reasonable time-averaged approximation to plume height for short-duration events, such as the initial Plinian and subplinian phases of the Hekla eruptions, but could potentially overestimate plume height (and consequently overestimate the MER) for eruptions of longer durations. Because MER scales with the fourth power of the column height, even small uncertainties in the former result in large uncertainties in the latter.

As seen from Fig. 6, the simplified approach of estimating MER from only the plume height, without considering the effect of wind and eruption temperature for these eruptions, yields MERs almost an order of magnitude lower. All the eruptions have scaling parameter Π in the range of 0.2–0.4, corresponding to transitional plumes, similar to those associated with the 18 May 1980 Mount St Helens eruption (Π 0.2–0.3) and the most powerful phases of both the 2010 Eyjafjallajökull and 2011 Cordón Caulle eruptions (Π 0.02–0.2). Π values of 0.2–0.4 indicate that the plume in these eruptions reached about 64–73 % of the height they would have reached in a wind-free environment (see Degruyter and Bonadonna 2012; Bonadonna et al. 2015b for more details).

Our critical analysis of the five largest historical Hekla eruptions has shown how ESPs cannot be assumed

deterministically based on single empirical strategies (e.g. Table 4). In fact, all empirical strategies (both for the determination of erupted volume and plume height) are sensitive to the deposit exposure in various manners, while the determination of MER strongly depends on the uncertainty in the determination of plume height (e.g. Biass et al. 2014a). A range of values for ESPs based on a critical analysis of tephra deposits (e.g. Table 4) can provide a more robust assessment of eruptive conditions than individual values based on arbitrary choices of empirical strategies. As already identified by the international community (e.g. Bonadonna et al. 2012), the use of a range of ESPs instead of single deterministic values has fundamental implication on tephra-dispersal forecasting that requires probabilistic treatments in order to compile comprehensive assessments.

Conclusions

The dispersal patterns of five of the 18 historical eruptions of Hekla volcano have been re-evaluated. The five eruptions are representative of the wider range of explosive eruptive behaviour observed at Hekla: eruptions in 1104 and 1158 had only a subplinian–Plinian phase and were of short duration, whereas those in 1693 and 1766 were similar to 20th century activity and started with a subplinian opening phase followed by weaker explosive activity and lava effusion over a prolonged time period. In contrast, the eruption in 1300 consisted of multiple higher-intensity, but probably short-lived, explosive phases. For the 1158, 1300, 1693, and 1766 eruptions, our new data (Table 4) result in larger volumes than previously estimated and imply higher plumes and MERs for the initial subplinian–Plinian phases than would be derived from the older estimates. The opening phase of the eruption in 1300 was of comparable intensity to the 1104 eruption. All plumes were probably transitional, with characteristics between those of strong and weak plumes.

The new volume estimates are comparable with, or larger than, previous estimates for four of the five eruptions (range of minimum values between 0.18 and 0.91 km^3; Table 3). We find that the volume range resulting from alternative placements or definition of the outermost isopach line (see Supplementary document 1) is greater than the range obtained from the choice of exponential segments, power-law or the Weibull function to describe the thinning rate of the deposit. Consequently, the outermost isopach line also has the largest influence on the volume-derived plume height and MER. The main uncertainty in the new volumes lies in the region of poorly constrained distal deposition. The well-constrained medial region of the deposit, which here is defined as the area between the most proximal isopach line and the 0.5-cm isopach line yields similar volumes for all methods of integration fit, whereas significant volume differences arise from the extrapolation beyond the isopach map into the poorly constrained proximal and distal fields.

These five eruptions are borderline between subplinian and Plinian in terms of MER (~10^7–10^8 kg s^{-1}) and plume heights, up to 25 km for the 1104 and 1300-D eruptions, up to 20 km for the 1158 eruption and up to 18 km for the 1693 and 1766 eruptions. These eruptions are five of the largest historical eruptions of Hekla. With the new estimates, the upper range of volumes observed for the four younger of these eruptions is increased. This has implications for hazards associated with future eruptions from Hekla. We also show the importance of accounting for atmospheric data and plume temperature in the calculation of MER, even for old eruptions for which the wind speed was not observed but can be retrieved from the method of Carey and Sparks (1986).

To define default ESPs to use for tephra-dispersal forecasting during future eruptions of Hekla, Mastin et al. (2009a, b) categorised Hekla as a type S2 volcano (medium sized silicic) which corresponds to typical plume heights of 6–12 km or VEI 3. This category is representative for the more recent, 20th to 21st century eruptions of Hekla, but not for all the historical activity. The five studied Hekla eruptions are all type S3 (large silicic), with plume heights equal or larger than 12 km or VEI 4 or higher (Table 4). For at least five of the last 18 eruptions of Hekla, the pre-assigned S2 category would thus have resulted in a serious underestimate of erupted mass and plume height. Extending the database for Hekla further, to the last 5000 years, would include at least eight S3 eruptions. Mastin et al. (2009b) assigned category S3, which is the highest on the general silicic scale, very restrictively. In fact, only one volcano was assigned this category, the reasoning being that many large (VEI 5) eruptions are preceded by smaller eruptions. For Hekla, the opposite is true, with the most powerful activity occurring in the first hour of the eruption.

The case of Hekla highlights the danger of considering a limited time range when assigning a pre-defined category for forecasting purposes. Volcanoes such as Hekla, which display a wide range in eruptive behaviour, are exceptionally hard to assign to a single category. In fact, before assessing a likely eruptive scenario a whole assessment of activity cycles should be carried out based on comprehensive datasets.

Acknowledgements This research was funded by the National Science Foundation grant EAR12-20596. The authors are grateful to Wim Degruyter for developing a dedicated and simple script for the calculation of MER. Special thanks to Kristine Curran, Carolyn Parcheta, Samantha Weaver, Jonas Gudnason, William Moreland, Catherine Gallagher and Jodi Fox for assistance with field work. The manuscript was significantly enhanced by insightful reviews by M. Nathenson and an anonymous reviewer, and comments from D. Swanson, S. Fagents and editor J. Fierstein.

References

Beckett FM, Witham CS, Hort MC, Stevenson JA, Bonadonna C, Millington SC (2015) Sensitivity of dispersion model forecasts of volcanic ash clouds to the physical characteristics of the particles. J Geophys Res-Atmos. doi:10.1002/2015JD023609

Biass S, Bagheri G, Aeberhard WH, Bonadonna C (2014a) TError: towards a better quantification of the uncertainty propagated during the characterization of tephra deposits. Statistics in Volcanology 1: 1–27. doi:10.5038/2163-338X.1.2

Biass S, Scaini C, Bonadonna C, Folch A, Smith K, Höskuldsson A (2014b) A multi-scale risk assessment for tephra fallout and airborne concentration from multiple Icelandic volcanoes- part 1: hazard assessment. Nat Hazard Earth Sys 14:2265–2287. doi:10.5194/nhess-14-2265-2014

Bonadonna C, Costa A (2012) Estimating the volume of tephra deposits: a new simple strategy. Geology 40:415–418. doi:10.1130/G32769.1

Bonadonna C, Costa A (2013) Plume height, volume, and classification of explosive volcanic eruptions based on the Weibull function. B Volcanol 75:742. doi:10.1007/s00445-013-0742-1

Bonadonna C, Houghton BF (2005) Total grain-size distribution and volume of tephra-fall deposits. B Volcanol 67:441–456. doi:10.1007/s00445-004-0386-2

Bonadonna C, Phillips JC (2003) Sedimentation from strong volcanic plumes. J Geophys Res-Sol Ea 108:2340–2368. doi:10.1029/2002JB002034

Bonadonna C, Ernst GGJ, Sparks RSJ (1998) Thickness variations and volume estimates of tephra fall deposits: the importance of particle Reynolds number. J Volcanol Geoth Res 81:173–187. doi:10.1016/S0377-0273(98)00007-9

Bonadonna C, Folch A, Loughlin S, Puempel H (2012) Future developments in modelling and monitoring of volcanic ash clouds: outcomes from the first IAVCEI-WMO workshop on Ash Dispersal Forecast and Civil Aviation (Geneva, Switzerland, 18–20 October 2010), Short Scientific Communication, Bulletin of Volcanology (http://www.springerlink.com/content/h01x16460482134w/)

Bonadonna C, Biass S, Costa A (2015a) Physical characterization of explosive volcanic eruptions based on tephra deposits: propagation of uncertainties and sensitivity analysis. J Volcanol Geoth Res 296: 80–100. doi:10.1016/j.jvolgeores.2015.03.009

Bonadonna C, Pistolesi M, Cioni R, Degruyter W, Elissondo M, Baumann V (2015b) Dynamics of wind-affected volcanic plumes: the example of the 2011 Cordón Caulle eruption, Chile. J Geophys Res-Sol Ea 120:2242–2261. doi:10.1002/2014JB011478

Burden RE, Chen L, Phillips JC (2013) A statistical method for determining the volume of volcanic fall deposits. B Volcanol 75:707. doi:10.1007/s00445-013-0707-4

Carey S, Sigurdsson H (1989) The intensity of plinian eruptions. B Volcanol 51:28–40. doi:10.1007/BF01086759

Carey S, Sparks RSJ (1986) Quantitative models for the fallout and dispersal of tephra from volcanic eruption columns. B Volcanol 48: 109–125. doi:10.1007/BF01046546

Carey RJ, Houghton BF, Thordarson T (2009) Tephra dispersal and eruption dynamics of wet and dry phases of the 1875 eruption of Askja volcano, Iceland. B Volcanol 72:259–278. doi:10.1007/s00445-009-0317-3

Cioni R, Longo A, Macedonio G, Santacroce R, Sbrana A, Sulpizio R, Andronico D (2003) Assessing pyroclastic fall hazard through field data and numerical simulations: example from Vesuvius. J Geophys Res-Sol Ea 108:2063. doi:10.1029/2001JB000642

Cooke MC, Francis PN, Millington S, Saunders R, Witham C (2014) Detection of the Grímsvötn 2011 volcanic eruption plumes using infrared satellite measurements. Atmos Sci Lett 15:321–327. doi:10.1002/asl2.506

Degruyter W, Bonadonna C (2012) Improving on mass flow rate estimates of volcanic eruptions. Geophys Res Lett 39:L16308. doi:10.1029/2012GL052566

Dugmore AJ, Church MJ, Mairs K-A, McGovern TH, Perdikaris S, Vesteinsson O (2007) Abandoned farms, volcanic impacts, and woodland management: revisiting Þjórsárdalur, the "Pompeii of Iceland. Arctic Anthropol 44:1–11. doi:10.1353/arc.2011.0021

Fierstein J, Nathenson M (1992) Another look at the calculation of fallout tephra volumes. B Volcanol 54:156–167. doi:10.1007/BF00278005

Folch A, Sulpizio R (2010) Evaluating long-range volcanic ash hazard using supercomputing facilities: application to Somma-Vesuvius (Italy), and consequences for civil aviation over the Central Mediterranean area. B Volcanol 72:1039–1059. doi:10.1007/s00445-010-0386-3

Gronvold K, Larsen G, Einarsson P, Thorarinsson S, Saemundsson K (1983) The Hekla eruption 1980–1981. B Volcanol 46:349–363. doi:10.1007/BF02597770

Gudmundsson A, Oskarsson N, Gronvold K, Saemundsson K, Sigurdsson O, Stefansson R, Gislason SR, Einarsson P, Brandsdottir B, Larsen G, Johannesson H, Thordarson T (1992) The 1991 eruption of Hekla, Iceland. B Volcanol 54:238–246. doi:10.1007/BF00278391

Gudmundsson MT, Höskuldsson A, Larsen G, Thordarson T, Oladottir BA, Oddsson B, Gudnason J, Högnadottir T, Stevenson JA, Houghton BF, McGarvie D, Sigurdardottir GM (2012) The may 2011 eruption of Grímsvötn. Geophys Res Abstr 14:EGU2012–EG12119

Höskuldsson Á, Óskarsson N, Pedersen R, Grönvold K, Vogfjörd K, Ólafsdottir R (2007) The millennium eruption of Hekla in February 2000. B Volcanol 70:169–182. doi:10.1007/s00445-007-0128-3

Houghton BF, Swanson DA, Rausch J, Carey RJ, Fagents SA, Orr TR (2013) Pushing the Volcanic Explosivity Index to its limit and beyond: constraints from exceptionally weak explosive eruptions at Kilauea in 2008. Geology 41:627–630. doi:10.1130/G34146.1

Jenkins S, McAneney J, Magill C, Blong R (2012) Regional ash fall hazard II: Asia-Pacific modelling results and implications. B Volcanol 74:1713–1727. doi:10.1007/s00445-012-0628-7

Klawonn M, Houghton BF, Swanson DA, Fagents SA, Wessel P, Wolfe CJ (2014a) Constraining explosive volcanism: subjective choices during estimates of eruption magnitude. B Volcanol 76:793. doi:10.1007/s00445-013-0793-3

Klawonn M, Houghton BF, Swanson DA, Fagents SA, Wessel P, Wolfe CJ (2014b) From field data to volumes: constraining uncertainties in pyroclastic eruption parameters. B Volcanol 76:839. doi:10.1007/s00445-014-0839-1

Larsen G (1992) Gjóskulagid úr Heklugosinu 1158 (The tephra layer from the 1158 AD eruption of Hekla). Jardfrædafélag Islands, Vorrádstefna, Yfirlit og Ágrip. Geoscience Society of Iceland, Reykjavík, pp 25–27

Larsen G, Thorarinsson S (1977) H4 and other acid Hekla tephra layers. Jokull 27:28–46

Larsen G, Dugmore A, Newton A (1999) Geochemistry of historical-age silicic tephras in Iceland. The Holocene 9:463–471. doi:10.1191/095968399669624108

Le Pennec J-L, Ruiz GA, Ramón P, Palacios E, Mothes P, Yepes H (2012) Impact of tephra falls on Andean communities: the influences of eruption size and weather conditions during the 1999–2001 activity of Tungurahua volcano, Ecuador. J Volcanol Geoth Res 217–218: 91–103. doi:10.1016/j.jvolgeores.2011.06.011

Mastin LG, Guffanti M, Ewert JE, Spiegel J (2009a) Preliminary spreadsheet of eruption source parameters for volcanoes of the world. U.S. Geological Survey Open-File Report 2009–1133, v. 1.2

Mastin LG, Guffanti M, Servranckx R, Webley P, Barsotti S, Dean K, Durant A, Ewert JW, Neri A, Rose WI, Schneider D, Siebert L, Stunder B, Swanson G, Tupper A, Volentik A, Waythomas CF

(2009b) A multidisciplinary effort to assign realistic source parameters to models of volcanic ash-cloud transport and dispersion during eruptions. J Volcanol Geoth Res 186:10–21. doi:10.1016/j.jvolgeores.2009.01.008

Petersen GN, Bjornsson H, Arason P, von Löwis S (2012) Two weather radar time series of the altitude of the volcanic plume during the May 2011 eruption of Grímsvötn, Iceland. Earth System Science Data 4:121–127. doi:10.5194/essd-4-121-2012

Pyle DM (1989) The thickness, volume and grainsize of tephra fall deposits. B Volcanol 51:1–15. doi:10.1007/BF01086757

Pyle DM (1995) Assessment of the minimum volume of tephra fall deposits. J Volcanol Geoth Res 69:379–382. doi:10.1016/0377-0273(95)00038-0

Scaini C, Biass S, Galderisi A, Bonadonna C, Folch A, Smith K, Höskuldsson A (2014) A multi-scale risk assessment for tephra fallout and airborne concentration from multiple Icelandic volcanoes—part 2: vulnerability and impact. Nat Hazard Earth Sys 14:2289–2312. doi:10.5194/nhess-14-2289-2014

Sturkell E, Ágústsson K, Linde AT, Sacks SI, Einarsson P, Sigmundsson F, Geirsson H, Pedersen R, LaFemina PC, Ólafsson H (2013) New insights into volcanic activity from strain and other deformation data for the Hekla 2000 eruption. J Volcanol Geoth Res 256:78–86. doi:10.1016/j.jvolgeores.2013.02.001

Thorarinsson S (1954) The tephra-fall from Hekla on March 29, 1947. In: Einarsson T, Kjartansson G, Thorarinsson S (eds) The eruption of Hekla 1947–1948. Societas Scientiarum Islandica, Reykjavík, pp. 1–68

Thorarinsson S (1967) The eruptions of Hekla in historical times: a tephrochronological study. In: Einarsson T, Kjartansson G, Thorarinsson S (eds) The eruption of Hekla 1947–1948. Societas Scientiarum Islandica, Reykjavík, pp. 1–177

Thordarson T, Höskuldsson Á (2008) Postglacial volcanism in Iceland. Jokull 58:197–228

Thordarson T, Larsen G (2007) Volcanism in Iceland in historical time: volcano types, eruption styles and eruptive history. J Geodyn 43:118–152. doi:10.1016/j.jog.2006.09.005

Walker GL (1973) Explosive volcanic eruptions—a new classification scheme. Geol Rundsch 62:431–446. doi:10.1007/BF01840108

Wilson L, Walker GPL (1987) Explosive volcanic eruptions—VI. Ejecta dispersal in Plinian eruptions: the control of eruption conditions and atmospheric properties. Geophys J Roy Astr S 89:657–679. doi:10.1111/j.1365-246X.1987.tb05186.x